Int. J. Nanosci. Nanotechnol., Vol. 16, No. 4, Dec. 2020, pp. 219-231

Gum Acacia/Carbopol-Based Biocomposites Loaded with Silver Nnanoparticles as Potential Wound Dressings

Rakgoshi Lekalakala[1], Blessing Atim Aderibigbe[2,*], Shesan John Owonubi[3], Emanuel Rotimi Sadiku[1], Youmbi Theirry Fonkui[4], Derek Tantoh Ndinteh[5] and Suprakas Sinha Ray[5, 6]

[1]Department of Polymer Technology, Tshwane University of Technology, Pretoria, South Africa.
[2]Department of Chemistry, University of Fort Hare, Alice Campus, Alice, South Africa.
[3]Department of Chemistry, University of Zululand, KwaDlangezwa, KwaZulu-Natal, South Africa.
[4]Department of Biotechnology and Food Technology, Faculty of Science, University of Johannesburg, Johannesburg, South Africa.
[5]Department of Applied Chemistry, University of Johannesburg, Doornfontein Campus, Johannesburg, South Africa.
[6]DST/CSIR National Centre for Nanostructured Materials, Council for Scientific and Industrial Research, Pretoria, South Africa.

(*) Corresponding author: blessinaderibigbe@gmail.com
(Received: 01 May 2020 and Accepted: 07 June 2020)

Abstract

Wounds infected with bacteria are treated using wound dressings loaded with antibiotics. However, the use of antibiotics has resulted in drug resistance. In order to overcome drug resistance common with most of the currently used antibiotics, several researchers have evaluated the potential of metal-based nanoparticles as antimicrobial agents. In this research, smart materials with good antibacterial activity were developed as potential wound dressings from a combination of bio- and synthetic polymers (gum acacia and carbopol, respectively) followed by loading with silver nanoparticles. The biocomposites were pH-sensitive with good water uptake. The hydrogels exhibited a high degree of swelling which increased with increase in pH. Their swelling capability was significant at pH of 7.4 simulating wound exudates. Their physicochemical properties were studied by FTIR, XRD, SEM and AFM. Furthermore, their antibacterial activity was significant against Gram-positive and Gram-negative strains of bacteria used in the study. The significant features of the biocomposites revealed their potential application as smart materials for the treatment of bacteria-infected and high exuding wounds.

Keywords: *Gum acacia, Carbopol, Silver nanoparticles, Neem bark extract, Antibacterial activity, Biocomposites.*

1. INTRODUCTION

Bacterial infections are common in damaged skin resulting from wounds [1]. A current study further indicated that a common bacterial pathogen, *Pseudomonas aeruginosa* partners with a virus to cause chronic wounds [1]. Bacteria infected wounds are treated with wound dressings loaded with antibiotics. However, the currently used conventional antibiotics suffer from serious pharmacological limitations such as drug resistance, poor water solubility and toxicity [2,3]. Due to the aforementioned limitations, several researchers have investigated metal-based nanoparticles as potential antimicrobial agents. Metal-based nanoparticles exhibit good antibacterial activity. The commonly studied nanoparticles are silver, titanium

dioxide, zinc oxide, gold nanoparticles etc. The unique feature that is responsible for their good antibacterial activity is their large surface area [4]. The antibacterial mechanisms of action of nanoparticles are speculated to be via the toxicity of free metal ion and by oxidative stress as a result of the production of reactive oxygen species on the nanoparticle surfaces [4, 5].

Wound dressings have been developed from biopolymers due to their unique features such as good hydrophilicity, biodegradability, permeability, biocompatibility, non-toxicity, non-immunogenic nature and the ease of surface modification [6,7]. However, their biomedical applications are limited by their poor mechanical properties, uncontrolled water uptake and varied properties that is dependent on the source [8,9]. Biopolymers which have been used in biomedical applications are chitosan, alginate, gum acacia, soy protein isolate, whey protein isolate, starch, cellulose *etc*. Gum acacia, a biopolymer content is dependent on its source and it is biodegradable with good surface activity [10,11]. Biopolymers are combined with synthetic polymers resulting in enhanced mechanical properties and controlled water uptake [12,13].

Synthetic polymers which have been employed in the development of wound dressings include carbopol etc. Carbopol belongs to the class of carbomers. It is pH-responsive with a high molecular weight composed of 50-60 % of acrylic acid groups. Some researchers prepared biocomposites from a combination of biopolymers and synthetic polymers loaded with silver nanoparticles as potential wound dressings with antibacterial activity. Alginate-based nanocomposites crosslinked with calcium carbonate and D-glucono-δ-lactone followed by loading with silver nanoparticles were effective against *E. coli* and *P. aeruginosa* strains of bacteria [14]. Chitosan/poly(vinyl alcohol)-based gels loaded with silver nanoparticles displayed good antibacterial activity and biocompatibility [15]. Chitosan-polyvinyl alcohol-based hydrogel loaded with silver nanoparticles exhibited good antibacterial activity [16]. Polyvinyl alcohol/gum acacia [17,18] and poly(vinyl alcohol)-sodium alginate-carboxymethylcellulose hydrogels loaded with silver nanoparticles exhibited good antibacterial activity [19].

The design of hybrid hydrogels loaded with in situ formation of silver nanoparticles was based on the hypothesis that they exhibit high water uptake, rough surfaces with good antibacterial activity. In this study, gum acacia/carbopol-based biocomposites loaded with silver nanoparticles prepared via *in situ* formation using neem bark extract were prepared. To the best of our knowledge, this is the first report on gum acacia/carbopol biocomposites containing silver nanoparticles. The biocomposites were characterized by Fourier Transform Infrared Spectroscopy (FTIR), Atomic Force Microscopy (AFM), X-ray Diffraction (XRD) and Scanning Electron Microscopy (SEM) followed by swelling and antibacterial analysis.

2. MATERIAL AND METHODS

2.1. Materials

N,N-methylenebisacrylamide (MBA) and acrylamide (AM), N,N,N,N - Tetramethylethylenediamine (TEMED), neem bark extract and potassium persulfate (KPS) were obtained from Merck Chemicals (South Africa). Gum acacia and silver nitrate were obtained from Total Lab, South Africa. Carbopol® 974P NF was obtained from Lubrizol, USA.

2.1.1. Preparation of the Biocomposites

Gum acacia was dissolved in 1 mL of distilled water and AM was added followed by the addition of MBA solution. The mixture was stirred to obtain a homogenous mixture. Carbopol was then added followed by KPS and TEMED (**Table 1**). The resultant mixture was stirred at room temperature until a

homogenous mixture was obtained. The biocomposites were formed at a temperature between 30 and 50 °C. The biocomposites were then soaked in distilled water overnight in order to get rid of the unreacted amine, before drying at ambient temperature for 5 days.

Table 1. *Composition of the hydrogel biocomposites.*

Biocomposites	*AM*	*MBA (65 mM)*	*TEMED (86 mM)*	*KPS (37 mM)*	*Gum acacia*	*Carbopol*
Blank	*1 g*	*1 mL*	*1 mL*	*1 mL*	-	-
Ag-1	*1 g*	*1 mL*	*1 mL*	*1 mL*	*0.5 g*	*0.05 g*
Ag-2	*1 g*	*1 mL*	*1 mL*	*1 mL*	*0.5 g*	*0.10 g*
Ag-3	*1 g*	*1 mL*	*1 mL*	*1 mL*	*0.5 g*	*0.15 g*

2.1.2. The Loading of the Biocomposites with Silver Nanoparticles

The biocomposites were transferred to 0.005 M solution of silver nitrate and left in the solution overnight. The hydrogels were then wiped with tissue and transferred to neem bark extract and left in the fridge for 2 h resulting in a colour change of the biocomposites to brown confirming the formation of silver nanoparticles.

2.2. Methods

2.2.1. FTIR

FTIR analysis was performed in the range of 4000-500 cm^{-1}. It was performed on (Perkin Elmer Spectrum 100 FTIR spectrometer). The sample was placed on the diamond sample surface of the machine. The number of scans used was 32 at a resolution of 4 cm^{-1}.

2.2.2. XRD

XRD was performed using (PANalyticalX'Pert PRO), Netherlands. It was performed at (Cu Ka radiation, k 5 0.1546 nm) running at 45 kV and 40 mA. This analysis was performed in order to evaluate the amorphous or crystalline state of the biocomposites and to confirm the loading of the nanoparticles into the biocomposites.

2.2.3. SEM

The biocomposites were sputtered with gold nanoparticle before SEM analysis using JEOL-JSM 7500F SEM. It was used to evaluate the surface morphology of the biocomposites.

2.2.4. AFM

The surface morphology of the hydrogel biocomposites was evaluated using Atomic Force Spectroscopy (AFM) Digital Instruments Nanoscope, Veeco, MMAFMLN-AM (Multimode) instrument, USA. The samples were scanned over a length of 5 µm to give a surface area of 25 μm^2. The experiment was performed at room temperature in a tapping mode using a probe (RTESPAW-300 model). The scan rate was set to 0.50 Hz, the amplitude set point ranged from 1.27 to 1.440 V and probe frequency in the range of 280-310 kHz for all the analysis. The height and phase images were obtained.

2.2.5. Swelling Analysis

50 mg of the dry biocomposite was placed in 25 mL of buffer solutions (1.2 or 7.4) at ambient temperature simulating acidic and wound exudates pH, respectively. The water uptake of the biocomposites was evaluated by allowing the biocomposites to swell in selected buffer solutions until an equilibrium swelling was reached over a period of 24 h. They were then removed and blotted gently with blotting paper to remove the overloaded water on the surface and weighed. The swelling ratio at equilibrium (ER) was calculated from equation (1):

$$Seq = \frac{W_s - W_t}{W_t} \quad (1)$$

W_s -weight of the biocomposite at equilibrium W_t -weight of the biocomposite before swelling. The swelling ratio, SR of the biocomposites was evaluated by immersing dry biocomposites 50 mg in 25 mL of selected buffer solution (pH 7.4 or 10) at ambient temperature. At an interval of 30 min, the biocomposite was removed from the buffer solutions and blotted gently with blotting paper and weighed. SR was calculated from equation 2:

$$SR = \frac{M_s - M_d}{M_d} \quad (2)$$

M_s is the weight of the biocomposite at time t. M_d is the weight of the dried biocomposite before swelling

2.2.6. In Vitro Antibacterial Analysis

Disc diffusion method was used to determine the antimicrobial activity of each compound. The test was carried out following the procedure recorded by Othman *et al*. with some minor changes [20]. Each sample (200 mg) was suspended in the corresponding volumes and tested against 12 bacterial strains. Gram positive bacteria include *Bacillus cereus* (**BC**) (ATCC10876), *B subtilis* (**BS**) (ATCC19659), *Enterococcus faecalis* (**EF**) (ATCC13047), *Mycobacterium smegmatis* (**MS**) (MC2155), and *S aureus* (**SA**) (ATCC25923). Gram negative bacteria: *Enterobacter cloacae* (**ECL**) (ATCC13047), *Escherischia coli* (**EC**) (ATCC25922), *Enterobacter aerogenes*, (**EA**) (ATCC13048) *Klebsiella oxytoca* (**KO**) (ATCC8724), *K pneumonia* (**KP**) (ATCC13882), *Proteus mirabilis* (**PM**) (ATCC7002) *and Pseudomonas aeruginosa* (**PA**) (ATCC27853).

3. RESULTS

3.1. FTIR

The blank biocomposite FTIR spectra revealed characteristic peaks at 3267 cm^{-1} for N-H stretch, for C-H stretch at 2955 cm^{-1}, for C=O stretch at 1644 cm^{-1}, for C-H stretch and at 1538 cm^{-1} (**Figure 1a**). FTIR spectrum of Ag-2 displayed characteristic peaks at 3343 cm^{-1} for N-H stretch, at 3192 cm^{-1} for aromatic C-H stretch, at 2925 and 2853 cm^{-1} for C-H stretch, at 1645 cm^{-1} for C=O stretch, at 1588 for N-H bending and at 1082 cm^{-1} for C-O-C stretch (**Figure 1b**). FTIR spectrum of Ag-3 and blank loaded with silver nanoparticles displayed characteristic peaks at 3267 cm^{-1} for N-H stretch, C-H stretch was visible at 2917 cm^{-1}, C=O stretch was found at 1658 cm^{-1} and N-H bending was visible at 1594 cm^{-1} (**Figure 1c**).

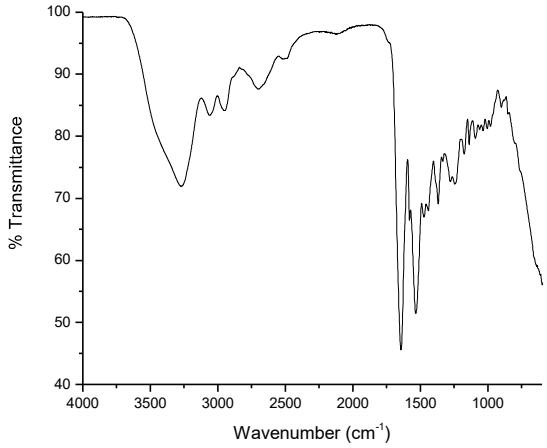

Figure 1a. *FTIR spectrum of blank biocomposites.*

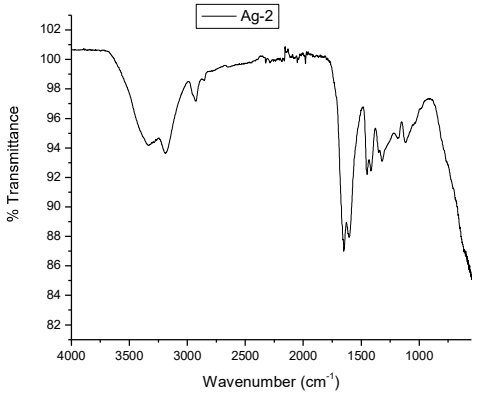

Figure 1b. *FTIR spectrum of Ag2 biocomposites.*

3.2. XRD

The XRD diffractograms of the blank biocomposite loaded with silver nanoparticles revealed a combination of a

broad peak at 22 ^{o} and sharp peaks at 29.34 ^{o}, 35.76 ^{o}, 38.26 ^{o}, 39.27 ^{o}, 42.93 ^{o}, 44.05 ^{o}, 47.32 ^{o}, 48.44 ^{o}, 56.37 ^{o} and 57.34^{o} (Figure 2a).

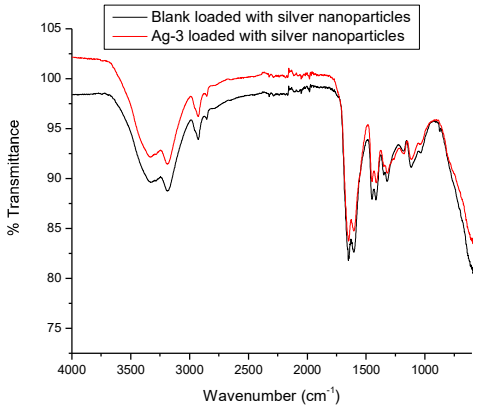

Figure 1c. *FTIR spectra of Ag3 and blank biocomposites loaded with Ag nanoparticles.*

The XRD diffractogram of **Ag1-3** loaded with silver nanoparticles also revealed a combination of a broad peak at 22 ^{o} and sharp peaks (**Figure 2b-d**). The sharp peaks on **Ag1** and **Ag2** were visible at 29.34 ^{o}, 38.52 ^{o}, 42.92 ^{o}, 44.17 ^{o}, 47.92 ^{o}, 48.44 ^{o}, and 57.36^{o}. However, **Ag3** displayed two distinct broad peaks at 22 and 44.04^{o} resulting from a high degree of crosslinking of the polymers (**Figure 2d**).

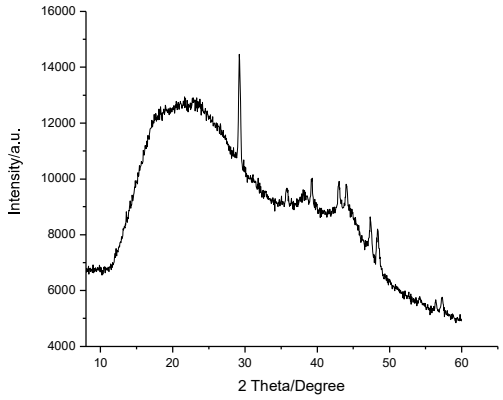

Figure 2a. XRD diffractograms of blank biocomposites.

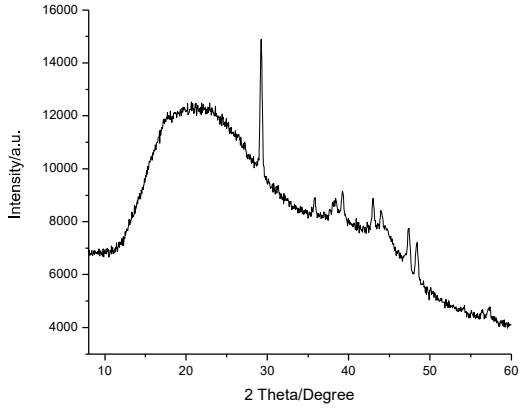

Figure 2b. XRD diffractograms of Ag1 biocomposite.

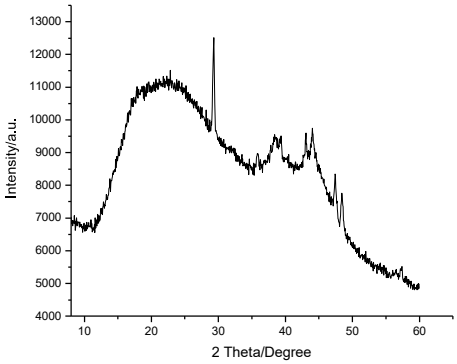

Figure 2c. XRD diffractogram of Ag2

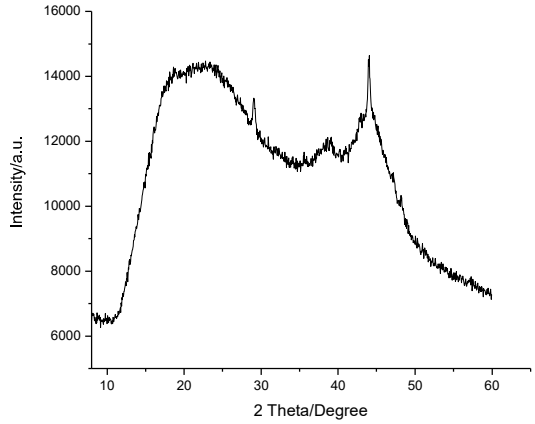

Figure 2d. XRD diffractogram of Ag3.

3.3. SEM

The blank SEM image was characterized by irregular morphology with a rough surface (**Figure 3a**). The morphology of biocomposite **Ag1** was similar to the blank (**Figure 3b**). However, there were pores which were significant when compared to the blank biocomposite. The morphology of **Ag2** was a combination of a smooth and rough surface (**Figure 3c**). The degree of roughness of the **Ag2** was enhanced resulting from the higher degree of crosslinking of the polymer when compared to **Ag1** and **Ag2**. The morphology of **Ag3** displayed a rough surface with irregular morphology (**Figure 3d**).

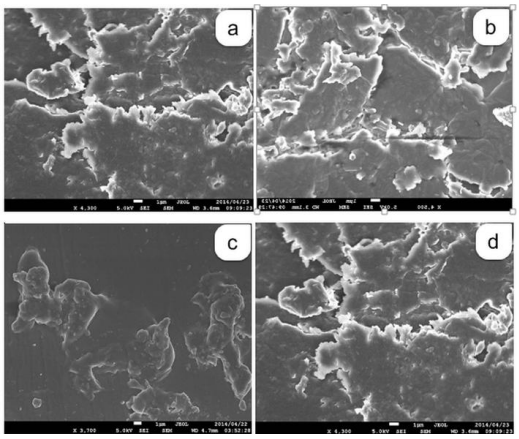

Figure 3. *SEM images (a) Blank biocomposites (b) Ag1 (c) Ag2 and (d) Ag3.*

3.4. AFM

The topography variations on the surface of the biocomposite was studied. (**Figure 4a-d**). The AFM images of the biocomposites revealed a high degree of roughness in **Ag3** when compared to the blank. However, **Ag2** biocomposite revealed a combination of a smooth and rough surfaces which similar to the SEM image. The WSxM software analysis of the biocomposites is shown in (**Table 2**) [21].

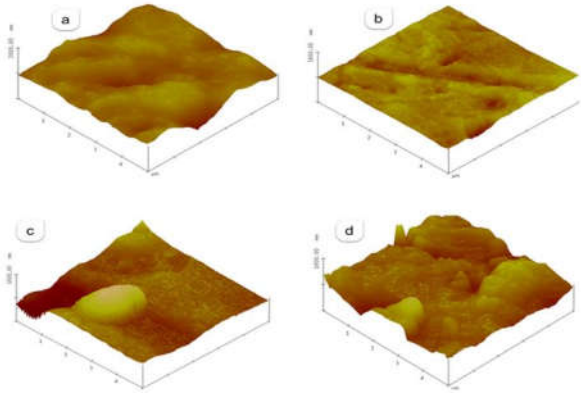

Figure 4. *AFM images (a) Blank biocomposites (b) Ag1 (c) Ag2 (d) Ag3.*

Table 2. *AFM analysis of the biocomposites using WSxM software.*

	Ag1	Ag2	Ag3	Blank
Roughness average	46.3524	49.6151	51.4176	44.9736
Root mean square	55.3259	59.2844	60.5385	54.6139
Surface skewness	-1.2509	-1.2496	-1.1874	-1.3264
Surface kurtosis	2.6697	2.7172	2.5414	3.0136
Average height	152.4043	150.5566	143.7547	151.2625

3.5. Swelling Property

Ag1-3 exhibited high swelling capability at pH 7.4 when compared to pH 1.2. The enhanced swelling capability of **Ag1-3** is attributed to the hydrophilic nature of gum acacia and carbopol (**Figure 5a & 5b**). The swelling capability of the biocomposites at acidic pH was low suggesting that they are pH-sensitive.

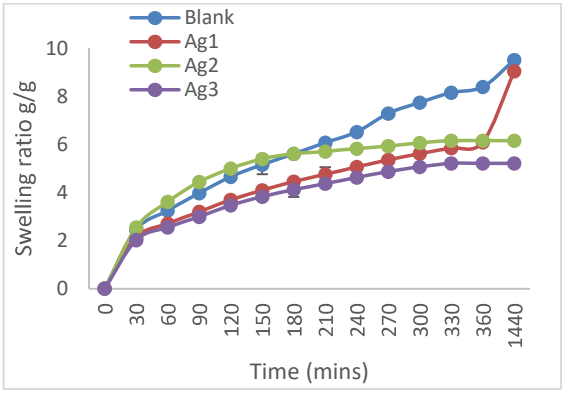

Figure 5a. *Swelling capacity of the biocomposites at pH 1.2.*

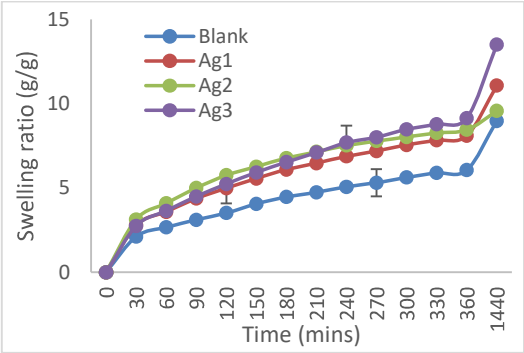

Figure 5b. *Swelling capacity of the biocomposites at pH 7.4.*

The water uptake kinetics of the hydrogel biocomposites were evaluated using equation 3.

$$M_{t/M_\infty} = Kt^n \quad (3)$$

Where M_t and M_∞ are the masses of the hydrogel biocomposites at time t and equilibrium, respectively. K is the diffusion constant of water into the hydrogel biocomposite matrices and n is the diffusion exponent.

Table 3. *Diffusion coefficient (D), diffusion exponent (n) and diffusion constant (K) of the biocomposites at pH 1.2 and 7.4.*

pH	Biocomposites	n	R^2	K	D	R^2
7.4	Blank	0.44	0.99	0.51	0.28	0.99
7.4	Ag-1	0.44	0.99	0.79	0.39	0.99
7.4	Ag-2	0.42	0.99	0.28	0.41	0.99
7.4	Ag-3	0.50	0.99	0.73	0.45	0.99
1.2	Blank	0.51	0.99	0.89	0.41	0.98
1.2	Ag-1	0.43	0.99	0.75	0.28	0.99
1.2	Ag-2	0.34	0.94	0.12	0.28	0.94
1.2	Ag-3	0.40	0.99	0.69	0.24	0.99

The n = 0.5 indicates case 1, which is a perfect Fickian process whereby the rate of network relaxation is faster than the rate of diffusion. When n = 1.0, it indicates a non-Fickian diffusion whereby water transport is controlled and the rate of diffusion is faster than the network relaxation. When 0.5 < n < 1.0, it indicates that the rate of penetrant mobility and segmental relaxation are comparable [22]. The slope of the graph of *ln* (M_t/M_∞) versus *ln* t for 60% swelling ratio determined the diffusion exponent, n of the biocomposites. The diffusion exponent values were found to be in a range of 0.34-0.51 indicating a combination of pseudo-Fickian and Fickian diffusion with a coefficient of determination of 0.99 indicating good linearity (**Table 3**). At pH 1.2, the n value of the blank biocomposite was 0.51 suggesting Fickian diffusion and the n values of **Ag1**, **Ag2**, **Ag3** were 0.43, 0.34 and 0.40, respectively indicating pseudo-Fickian diffusion. At pH 7.4, the n values of blank, **Ag1**, **Ag2** were 0.44, 0.44, 0.42 respectively indicating pseudo-Fickian diffusion and **Ag3** was 0.5 suggesting Fickian diffusion. The hydrogels diffusion coefficients were also calculated using equation 4.

$$S = 4\left[\frac{D}{\pi r^2}\right] 1/2\ {}_t 1/2 \quad (4)$$

where D, r, S, and t represent the diffusion coefficient, radius, fractional swelling of the hydrogels and time, respectively. To investigate the diffusion coefficient, D of the biocomposites, a graph of S versus $t^{1/2}$ were drawn and the diffusion coefficients were obtained from the slopes of these graphs. The diffusion coefficient was found to be between 0.24-0.45 respectively (**Table 3**). The coefficient of determination was in a range of 0.98-0.99 indicating good linearity.

3.6. In Vitro Antibacterial Analysis

The biocomposites were effective against gram-positive and gram-negative bacteria (**Table 4**). **Ag3** biocomposites exhibited enhanced antibacterial activity against *Bacillus cereus, Enterobacter cloacae* and

Pseudomonas aeruginosa. The biocomposites were also effective against *K pneumonia, Mycobacterium smegmatis and Pseudomonas aeruginosa* when compared to the neem bark extract. However, the biocomposites were not effective against *Klebsiella oxytoca* and *Proteus mirabilis* revealing the selective antibacterial activity of the biocomposites against some strains of bacteria. **Ag2** was effective against *Proteus mirabilis* when compared to **Ag1** and **Ag3**.

Table 4. *Antibacterial results of the biocomposites.*

Biocomposites	Bacterial strains with diameter of inhibition (mm)											
	EA	**EF**	**SA**	**BS**	**EC**	**BC**	**ECL**	**KO**	**PA**	**KP**	**MS**	**PM**
Ag-1	9	8	7	8	9	9	9	~	8	9	9	~
Ag-2	8	9	7	7	9	10	9	~	8	8	9	8
Ag-3	8	8	7	9	9	10	10	~	12	8	9	~
Neem bark extract	9	9	~	8	~	~	8	8	~	~	~	~

4. DISCUSSION

Gum acacia/carbopol-based bio-composites were prepared by free-radical polymerization and loaded with silver nanoparticles. Neem bark extract was used as a reducing agent and this approach was employed in order to enhance the antibacterial efficacy of the biocomposites. Some researchers used neem extract as a reducing agent [23,24]. Neem leaf extract was used as a capping and reducing agent. The nanoparticles prepared were effective against gram-positive and gram-negative bacteria [23, 25, 26]. Natural extracts are eco-friendly, cost-effective and useful for the preparation of silver nanoparticles [27-30]. The formation of the nanoparticles was performed in situ in the prepared biocomposites. The bicomposites serve as a potential reservoir for the sustained release of silver ions to promote wound healing. The in situ formation of the nanoparticle in the biocomposites was due to the reduction of Ag^{+} silver to Ag^{o} by the reducing agent, $NaBH_4$ [31,32]. This method promotes the formation of monodispersed silver nanoparticles within the matrices of the biocomposites [33,34].
The biocomposites were prepared by free-radical polymerization in which the hydroxyl group on the gum acacia was useful for crosslinking with the functional groups on the carbopol. Free radical polymerization is the most commonly used cross-linking technique. It offers several advantages such as it is very reactive resulting in high density of cross-linking density, it is appropriate for different functional groups and it occurs under mild conditions [35,36].

The FTIR spectra of the biocomposites revealed characteristic peaks of C-O-C stretch confirming the successful crosslinking of gum acacia in the hydrogel matrix [37,38]. The signal for the carbonyl group was significant at 1658 and 1645 cm^{-1} in the biocomposites due to carbopol crosslinked in the hydrogel matrix [38,39]. The FTIR further revealed the non-interaction of the loaded nanoparticles with the biocomposites network indicating the stability of the nanoparticles in the biocomposites. Biocomposites are good drug delivery systems and they have been employed for the delivery of silver nanoparticles [40-42]. Biocomposites exhibit some unique features making them useful systems for drug delivery such as they can be tailored for sustained and controlled drug release mechanism, exhibit high drug loading capacity, they are biocompatible and non-toxic [43-45].

The XRD diffractograms of the bicomposites loaded with silver nanoparticles displayed a combination of broad and sharp peaks confirming the successful loading of silver nanoparticles in the biocomposites. The broad peaks are due to the amorphous nature of the biocomposites resulting from the

crosslinking of the polymers. The sharp peaks are due to the Ag^o with face-centred cubic crystal structure nanoparticles in the biocomposites [46-48].

The SEM images of the blank biocomposite and **Ag1** was irregular with a rough surface morphology (**Figure 3a**). However, the significant pores on **Ag1** when compared to the blank biocomposite is attributed to the crosslinking of gum acacia with carbopol. The morphology of **Ag2** was a combination of a smooth and rough surface (**Figure 3c**). The degree of roughness of the **Ag3** was enhanced resulting from the higher degree of crosslinking of the polymer when compared to **Ag1** and **Ag2**. The SEM images revealed the presence of cavities suitable for high water uptake suggesting their capability to exhibit high swelling with enhanced permeability [38, 49]. Furthermore, the AFM images confirmed the rough surface of the biocomposites (**Figure 4a-d**). Their rough surface is attributed to their degree of crosslinking [50,51]. The rough surfaces of the biocomposites are suitable for accelerating cell adhesion, proliferation, and skin regeneration and these features have been reported to be important in wound dressings that can accelerate wound healing by some researchers [52,53]. The rough surfaces display a high surface area and they are excellent platform for cells that induce fibroblast adhesion [52-54]. Furthermore, the nature of surface of the biocomposites also promote their good adhesiveness making them potential materials for topical application at the wound surface [54]. The presence of cavities in the dressing materials also promote the permeation of atmospheric oxygen to the wound which is useful for accelerated wound healing [55-57].

The water uptake of the biocomposites reveals their capability to absorb wound exudate and maintain a moist environment at the wound bed. The blank hydrogel swelling capability at pH 7.4 was low when compared to **Ag1-3**. The aforementioned finding indicates that the presence of gum acacia and carbopol in the biocomposite play an important role in the swelling capability of the biocomposites. Carbopol and gum acacia contain hydrophilic functional groups that contribute to the swelling capacity of the biocomposites [58]. However, the blank hydrogel exhibited high swelling capability at pH 1.2 when compared to pH 7.4 revealing the pH sensitivity of the biocomposites [17]. The mechanism of water uptake into the biocomposites revealed that the diffusion exponent values were in a range of 0.34-0.51 indicating a combination of pseudo-Fickian and Fickian diffusion. The high water uptake of the biocomposites reveal their exudate drainage ability which is relative to their ability to absorb body fluids, transform cell nutrients, and provide a moist environment suitable for accelerated wound healing. Furthermore, the capability of the biocomposites to absorb exudates also protect the wound from microbial invasion which is usually responsible for chronic wound infections and also prevent wound drying thereby alleviating pains [55, 59].

The biocomposites antibacterial activity against *Bacllius cereus, Enterobacter clocae* and *P. aeruginosa* was significant for **Ag3** when compared to other biocomposites suggesting that the degree of crosslinking of the biocomposites influenced their selective antibacterial activity against selected strains of bacteria. The three aforementioned strains of bacteria have been reported to be responsible for infection in wounds [60,61]. Co-infection of *P. aeruginosa* and *S. aureus* can result in worse patient outcomes when compared to a single infection [62]. The biocomposites were also effective against *K pneumonia, Mycobacterium smegmatis and Pseudomonas aeruginosa* when compared to the neem bark extract. However, the biocomposites were not effective against *Klebsiella oxytoca* and *Proteus mirabilis* revealing the selective antibacterial activity

of the biocomposites against some strains of bacteria. Biocomposites **Ag2** was effective against *Proteus mirabilis* when compared to **Ag1** and **Ag3**. *Proteus mirabilis* is a common gram-negative pathogen found in clinical specimens. It is responsible for hospital and community-acquired infections such as infections in wounds, urinary tract and bloodstream infections [63,64]. This strain of bacteria is resistant to some classes of antibiotics which include tetracycline and nitrofurantoin. Ag2 was characterized by a combination of smooth and rough surfaces which could have also contributed to the significant antibacterial activity of Ag2 [65,66]. The high antibacterial activity of the biocomposites further confirmed the good dispersion of the silver nanoparticles in the biocomposites [67]. Silver nanoparticles penetrate bacterial cell wall causing structural changes on the cell membrane resulting in the nanoparticles accumulating on the cell surface [68,69]. Silver nanoparticles also act on bacteria by the formation of free radicals that damage the cell membrane making it porous thereby leading to cell death [68,69]. Silver ions released by silver nanoparticles inhibit several functions in the cell leading to cell death. It interacts with the sulfur and phosphorus of the bacteria DNA hindering the DNA replication of the bacteria. Another mode of action of silver nanoparticles have been reported to be via inhibition of signal transduction in bacteria by dephosphorylation of the peptide substrates on the tyrosine residues [70]. The results obtained in this study support our hypothesis that crosslinking gum acacia with carbopol enhance the water uptake, promote in situ formation of silver nanoparticles resulting in significant antibacterial activity against Gram-negative and Gram-positive strain of bacteria.

5. CONCLUSION

The biocomposites exhibited high water uptake at pH 7.4 when compared to pH 1.2. The highly crosslinked biocomposite, Ag3 exhibited a high degree of swelling when compared to other biocomposites.

The FTIR spectra revealed characteristic peaks confirming the successful crosslinking of gum acacia in the biocomposites. Their SEM images was a combination of irregular morphologies with rough surface and cavities which was influenced by the degree of crosslinking. The XRD diffractograms of the biocomposites displayed crystalline peaks of silver nanoparticles confirming the successful incorporation of the nanoparticles *in situ*. The antibacterial activity of the biocomposites was significant and selective against gram-positive and gram-negative strains of bacteria. The unique features of the biocomposites such as high water uptake, rough surfaces with cavities and good antibacterial activity suggest that they are potential wound dressings for accelerated wound healing.

ACKNOWLEDGEMENTS

The financial assistance of National Research Foundation and Medical Research Council (Self-Initiated Research), South Africa towards this research are hereby acknowledged. The views and opinions expressed in this manuscript are those of the authors and not of MRC or NRF.

CONFLICT OF INTEREST

The authors declare no conflict of interest.

REFERENCES

1. Sweere, J. M., Van Belleghem, J.D., Ishak, H., Bach, M.S., Popescu, M., Sunkari, V., Kaber, G., Manasherob, R., Suh, G. A., Cao, X., de Vries, C. R., "Bacteriophage trigger antiviral immunity and prevent clearance of bacterial infection", *Science*., 363 (2019) 6434-6465.
2. Heta, S., Robo, I., "The side effects of the most commonly used group of antibiotics in periodontal treatments". *Med. Sci.*, 6 (2018) 1-6.

3. Shono, Y., Docampo, M. D, Peled, J. U., Perobelli, S. M., Velardi, E., Tsai, J. J., Slingerland, A. E., Smith, O. M., Young, L. F., Gupta, J., Lieberman, S. R., "Increased GVHD-related mortality with broad-spectrum antibiotic use after allogeneic hematopoietic stem cell transplantation in human patients and mice". *Sci. Transl. Med.,* 8 (2016) 339-354
4. Owonubi, S. J., Ateba, C. N., & Revaprasadu, N., "Co-assembled ZnO-Fe_2O_{3x}-CuO_x nano-oxide materials for antibacterial protection". *Phosphorus, Sulfur.*, 196 (2020) 1-7.
5. Besinis, A., De Peralta, T., Handy, R. D., "The antibacterial effects of silver, titanium dioxide and silica dioxide nanoparticles compared to the dental disinfectant chlorhexidine on Streptococcus mutans using a suite of bioassays". *Nanotoxicology*., 8 (2014) 1-6.
6. Arora, D., Sharma, N., Sharma, V., Abrol, V., Shankar, R., Jaglan, S., "An update on polysaccharide-based nanomaterials for antimicrobial applications". *Appl. Microbiol. Biotechnol*., 100 (2016) 2603-2615.
7. Jung, G., Qin, Z., Buehler, M. J., "Mechanical properties and failure of biopolymers: atomistic reactions to macroscale response", Springer, Cham, (2015).
8. Basu, A., Kunduru, K. R., Abtew, E., Domb, A. J., "Polysaccharide-based conjugates for biomedical applications". *Bioconjug. Chem.,* 26 (2015) 1396-1412.
9. Shelke, N. B., James, R., Laurencin, C. T, Kumbar, S. G., "Polysaccharide biomaterials for drug delivery and regenerative engineering". *Polym. Adv. Technol.,* 25 (2014) 448-60.
10. Li, C., Zhu, B., Xue, H., Chen, Z., Ding, Q., Wang, X., "Physicochemical properties of dry-heated peanut protein isolate conjugated with dextran or gum Arabic". *J. Am. Oil. Chem. Soc.,* 90 (2013) 1801-1807.
11. Williams, P., Idris, O., Phillips, G., "Structural analysis of gum from Acacia senegal (gum arabic)", Springer, Boston, MA, (2000).
12. El-Hefian, E. A., Nasef, M. M., Yahaya, A. H., "Chitosan-based polymer blends: Current status and applications". *J. Chem. Soc. Pak.,* 36 (2014) 11.
13. Oh, S. H, Lee, J. H., "Hydrophilization of synthetic biodegradable polymer scaffolds for improved cell/tissue compatibility". *Biomed. Mater.*, 8 (2013) 014101.
14. Rescignano, N., Hernandez, R., Lopez, L. D., Calvillo, I., Kenny, J. M., Mijangos, C., "Preparation of alginate hydrogels containing silver nanoparticles: a facile approach for antibacterial applications". *Polym. Int.* 65 (2016) 921-926.
15. Hiep, N. T., Khon, H. C., Niem, V. V., Toi, V. V., Tran, N. Q., Hai, N. D., Mai, N, T., (2016) "Microwave-assisted synthesis of chitosan/polyvinyl alcohol silver nanoparticles gel for wound dressing applications"., *Int. J. Polym. Sci*., (2016), 1584046.
16. Agnihotri, S., Mukherji, S., Mukherji, S., "Antimicrobial chitosan–PVA hydrogel as a nanoreactor and immobilizing matrix for silver nanoparticles". *Appl. Nanosci*., 2 (2012) 179-88.
17. Juby, K. A., Dwivedi, C., Kumar, M., Kota, S., Misra, H. S., Bajaj, P. N., Silver nanoparticle-loaded PVA/gum acacia hydrogel: Synthesis, characterization and antibacterial study. *Carbohydr Polym*., 89 (2012) 906-13.
18. Li, M., Jiang, X., Wang, D., Xu, Z., Yang, M., "In situ reduction of silver nanoparticles in the lignin based hydrogel for enhanced antibacterial application". *Colloids. Surf. B. Biointerfaces.,* 177 (2019).370-376.
19. Chen, K., Wang, F., Liu, S., Wu, X., Xu, L., Zhang, D., "In situ reduction of silver nanoparticles by sodium alginate to obtain silver-loaded composite wound dressing with enhanced mechanical and antimicrobial property". *Int. J. Biol. Macromol.,* 148 (2020) 501-509.
20. Othman, M., Loh, S. H., Wiart, C., Khoo, T. J., Lim, K. H., Ting, K. N., "Optimal methods for evaluating antimicrobial activities from plant extracts". *J. Microbiol. Methods.*, 84 (2011) 161-166.
21. Horcas, I., Fernández, R., Gomez-Rodriguez, J. M., Colchero, J. W., Gómez-Herrero, J. W., Baro, A. M., "WSXM: a software for scanning probe microscopy and a tool for nanotechnology". *Rev. Sci. Instrum.* 78 (2007) 013705.
22. Ritger, P. L., Peppas, N. A., "A simple equation for description of solute release I. Fickian and non-fickian release from non-swellable devices in the form of slabs, spheres, cylinders or discs". *J. Control. Release,* 5 (1987) 23-36.
23. Renugadevi, K., Aswini, R. V., "Microwave irradiation assisted synthesis of silver nanoparticle using Azadirachta indica leaf extract as a reducing agent and in vitro evaluation of its antibacterial and anticancer activity". *Int. J. Nanomat. Bio.*, 2 (2012) 5-10.
24. Verma, A., Mehata, M. S., "Controllable synthesis of silver nanoparticles using Neem leaves and their antimicrobial activity". *J. Radiat. Res. Appl. Sci.,* 9 (2016) 109-115.
25. Ahmed, S., Saifullah, Ahmad, M., Swami, B. L., Ikram, S., "Green synthesis of silver nanoparticles using Azadirachta indica aqueous leaf extract". *Radiat. Res. Appl. Sci.,* 9 (2016) 1-7.
26. Roy, P., Das, B., Mohanty, A., Mohapatra, S., "Green synthesis of silver nanoparticles using Azadirachta indica leaf extract and its antimicrobial study". *Appl. Nanosci.,* 7 (2017) 843-850.
27. Lima, A.K., Vasconcelos, A. A., Sousa Júnior, J. J., Escher, S. K., Nakazato, G., Taube Júnior, P. S., "Green Synthesis of Silver NanoparticlesUsing Amazon Fruits ". *Int. J. Nanosci. Nanotechnol*., 15 (2019) 179-188.

28. Paseban, N., Ghadam, P., Pourhosseini, P. S., "The Fluorescence Behavior and Stabilityof AgNPs Synthesized by Juglans RegiaExtract Green Husk Aqueous ". *Int. J. Nanosci. Nanotechnol*., 15 (2019) 117-126.
29. Kurian, M., Varghese, B., Athira, T. S., Krishna, S., "Novel and efficient synthesis of silver nanoparticles using curcuma longa and zingiber officinale rhizome extracts". *Int. J. Nanosci. Nanotechnol*., 12 (2016) 175-181.
30. Mittal, D., Narang, K., Leekha, A., Kapinder, K., Verma A. K., "Elucidation of Biological Activity of Silver Based Nanoparticles Using Plant Constituents of *Syzygium cumini"*. *Int. J. Nanosci. Nanotechnol*., 15 (2019) 189-198.
31. Kora, A. J., Sashidhar, R. B., Arunachalam, J., "Gum kondagogu (*Cochlospermum gossypium*): A template for the green synthesis and stabilization of silver nanoparticles with antibacterial application". *Carbohydr. Polym.,* 82 (2010) 670–679.
32. Lustosa, A. K, de Jesus Oliveira, A. C., Quelemes, P. V., Plácido, A., Da Silva, F. V., Oliveira I. S., De Almeida, M. P., Amorim, A. D., Delerue-Matos, C., De Oliveira, R. D., Da Silva, D. A., "In situ synthesis of silver nanoparticles in a hydrogel of carboxymethyl cellulose with phthalated-cashew gum as a promising antibacterial and healing agent". *Int. J. Mol. Sci.*, 18 (2017) 2399.
33. Reithofer, M. R., Lakshmanan, A., Ping, A. T., Chin, J. M., Hauser, C. A., "In situ synthesis of size-controlled, stable silver nanoparticles within ultrashort peptide hydrogels and their anti-bacterial properties". *Biomaterials*., 35 (2014) 7535-7542.
34. GhavamiNejad, A., Park, C. H., Kim, C. S., "In situ synthesis of antimicrobial silver nanoparticles within antifouling zwitterionic hydrogels by catecholic redox chemistry for wound healing application". *Biomacromolecules,* 17 (2016) 1213-1223.
35. Bi, X., Liang, A., "In Situ-Forming Cross-linking Hydrogel Systems: Chemistry and Biomedical Applications, Emerging Concepts in Analysis and Applications of Hydrogels". IntechOpen, United Kingdom, (2016).
36. Matyjaszewski, K., Spanswick, J., "Controlled/living radical polymerization". *Mater. Today,* 8 (2005) 26–33.
37. Patel, P. K., Pandya, S. S., "Preparation and Characterization of Crosslinked Gum Acacia Microspheres by Single Step Emulsion In-Situ Polymer Crosslinking Method: A Potential Vehicle for Controlled Drug Delivery". *Res. Rev. J. Pharm. Pharm. Sci.,* 2 (2013) 40-48.
38. Singh, B., Dhiman, A., "Design of Acacia gum–carbopol–cross-linked-polyvinylimidazole hydrogel wound dressings for antibiotic/anesthetic drug delivery". *Ind. Eng. Chem. Res.*, 55 (2016) 9176-9188.
39. Khandai, M., Chakraborty, S., Ghosh, A. K., "Critical analysis of algino-carbopol multiparticulate system for the improvement of flowability, compressibility and tableting properties of a poor flow drug". *Powder Technol*., 253 (2014) 223-229.
40. Ahamed, M. N., Sankar, S., Kashif, P. M., Basha, S. H., Sastry, T. P., "Evaluation of biomaterial containing regenerated cellulose and chitosan incorporated with silver nanoparticles". *Int. J. Biol. Macromol.,* 72 (2015) 680-686.
41. Prusty, K., Swain, S. K., "Nano silver decorated polyacrylamide/dextran nanohydrogels hybrid composites for drug delivery applications". *Mater. Sci. Eng. C*. 85 (2018) 130-141.
42. Wu, J., Zheng, Y., Song, W., Luan, J., Wen, X., Wu, Z., Chen, X., Wang, Q., Guo, S., "In situ synthesis of silver-nanoparticles/bacterial cellulose composites for slow-released antimicrobial wound dressing". *Carbohydr. Polym.,* 102 (2014) 762-771.
43. Harris, M., Ahmed, H., Barr, B., LeVine, D., Pace, L., Mohapatra, A., Morshed, B., Bumgardner, J. D., Jennings, J. A., "Magnetic stimuli-responsive chitosan-based drug delivery biocomposite for multiple triggered release". *Int. J. Biol. Macromol.* 104 (2017) 1407-1414.
44. Bera, H., Abbasi, Y. F., Yoke, F. F., Seng, P. M., Kakoti, B. B., Ahmmed, S. M., Bhatnagar, P., "Ziprasidone-loaded arabic gum modified montmorillonite-tailor-made pectin based gastroretentive composites". *Int. J. Biol. Macromol.*, 129 (2019) 552-563.
45. Padmanabhan, V. P., Kulandaivelu, R., Nellaiappan, S. N., "New core-shell hydroxyapatite/Gum-Acacia nanocomposites for drug delivery and tissue engineering applications". *Mater. Sci. Eng. C*., 92 (2018) 685-693.
46. Berdous, D., Ferfera-Harrar, H., "Green synthesis of nanosilver-loaded hydrogel nanocomposites for antibacterial application". *Int. J. Pharmacol. Pharm. Sci.* 10 (2016) 543-50.
47. Bajpai, S. K., Bajpai, M., Sharma, L., "In situ formation of silver nanoparticles in poly (N-isopropyl acrylamide) hydrogel for antibacterial applications". *Des. Monomers. Polym.* 14 (2011) 383-394.
48. Bajpai, S. K., Kumari, M., "A green approach to prepare silver nanoparticles loaded gum acacia/poly (acrylate) hydrogels". *Int. J. Biol. Macromol.* 80 (2015) 177-188.

49. Li, L., Wang, N., Jin, X., Deng, R., Nie, S., Sun, L., Wu, Q., Wei, Y., Gong, C., "Biodegradable and injectable in situ cross-linking chitosan-hyaluronic acid based hydrogels for postoperative adhesion prevention". *Biomaterials,* 35 (2014) 3903-3917.
50. Oprea, S., Oprea, V., "Synthesis and characterization of the cross-linked polyurethane–gum arabic blends obtained by multiacrylates cross-linking polymerization". *J. Elastom. Plast.,* 45 (2013) 564-576.
51. Hindi, S. S., Albureikan, M. O., Al-Ghamdi, A. A. , Alhummiany, H., Ansari, M. S., "Synthesis, characterization and biodegradation of gum Arabic-based bioplastic membranes". *Nanosci. Nanotechnol*. 4 (2017) 32-42.
52. Alves, A., Miguel, S. P., Araujo, A. R., de Jesús Valle, M. J., Sánchez Navarro, A., Correia, I. J., Ribeiro M. P., Coutinho, P., "Xanthan Gum–Konjac Glucomannan Blend Hydrogel for Wound Healing". *Polymers*, 12 (2020) 1-15.
53. Ribeiro, M. P., Morgado, P. I., Miguel, S. P., Coutinho, P., Correia, I. J., "Dextran-based hydrogel containing chitosan microparticles loaded with growth factors to be used in wound healing". *Mater. Sci. Eng. C.* 33 (2013) 2958-2966.
54. Thangavel, P., Ramachandran, B., Chakraborty, S., Kannan, R., Lonchin, S., Muthuvijayan, V., "Accelerated healing of diabetic wounds treated with l-glutamic acid loaded hydrogels through enhanced collagen deposition and angiogenesis: an in vivo study". *Sci Rep.*7 (2017) 1-5.
55. Li, Y., Jiang, H., Zheng, W., Gong, N., Chen, L., Jiang, X., Yang, G., "Bacterial cellulose–hyaluronan nanocomposite biomaterials as wound dressings for severe skin injury repair". *J. Mater. Chem. B.*, 3 (2015) 3498-3507.
56. Zheng, A., Xue, Y., Wei, D., Li, S., Xiao H, Guan Y., "Synthesis and characterization of antimicrobial polyvinyl pyrrolidone hydrogel as wound dressing". *Soft Mater*. 12 (2014) 179-187.
57. Desphande, D. S., Bajpai, R., Bajpai, A. K., "Water sorption and biocompatibility evaluation of poly(vinyl alcohol-acrylonitrile) based hydrogels". *Soft Mater,* 11 (2013) 221–230.
58. Hamzavi, N., Dewavrin, J. Y., Drozdov, A. D., Birgersson, E., "Nonmonotonic swelling of agarose-carbopol hybrid hydrogel: Experimental and theoretical analysis". *J. Polym. Sci. Pol. Phys.* 55 (2017) 444-454.
59. Wang, Y., Li, P., Xiang, P., Lu, J., Yuan, J., Shen, J., "Electrospun polyurethane/keratin/AgNP biocomposite mats for biocompatible and antibacterial wound dressings". *J. Mater. Chem. B.*, 4 (2016) 635-648.
60. Kim, M., Christley, S., Khodarev, N. N., Fleming, I., Huang, Y., Chang, E., Zaborina, O., Alverdy, J., "Pseudomonas aeruginosa wound infection involves activation of its iron acquisition system in response to fascial contact". *J. Trauma Acute Care Surg.,* 78 (2015) 823.
61. Michelotti, F., Bodansky, H. J., "Bacillus cereus causing widespread necrotising skin infection in a diabetic person". *Pract Diabetes*, 32 (2015) 169-170a.
62. DeLeon, S., Clinton, A., Fowler, H., Everett, J., Horswill, A. R., Rumbaugh, K. P., "Synergistic interactions of Pseudomonas aeruginosa and Staphylococcus aureus in an *in vitro* wound model". *Infect immune*. 82 (2014) 4718-4728.
63. Endimiani, A., Luzzaro, F., Brigante, G., Perilli, M., Lombardi, G., Amicosante, G., Rossolini, G. M., Toniolo, A., "Proteus mirabilis bloodstream infections: risk factors and treatment outcome related to the expression of extended-spectrum β-lactamases". *Antimicrob. Agents Chemother.* 49 (2005) 2598-2605.
64. Wang, J. T., Chen, P. C., Chang, S. C., Shiau, Y. R., Wang, H. Y., Lai, J. F., Huang, I. W., Tan, M. C., Lauderdale, T. L., "Antimicrobial susceptibilities of Proteus mirabilis: a longitudinal nationwide study from the Taiwan surveillance of antimicrobial resistance (TSAR) program". *BMC Infect. Dis.* 4 (2014) 486.
65. Jamshidi, D., Sazegar, M. R., "Antibacterial Activity of a Novel Biocomposite Chitosan/Graphite Based on Zinc-Grafted Mesoporous Silica Nanoparticles". *Int. J. Nanomed.* 15 (2020) 871-883.
66. Luan, Y., Liu, S., Pihl, M., van der Mei, H. C., Liu, J., Hizal, F., Choi, C. H., Chen, H., Ren, Y., Busscher, H. J., "Bacterial interactions with nanostructured surfaces". *Curr. Opin. Colloid Interface Sci.* 38 (2018) 170-189.
67. Rodríguez Nuñez, Y. A., Castro, R. I., Arenas, F. A., López-Cabaña, Z. E., Carreño, G., Carrasco-Sánchez, V., Marican, A., Villaseñor, J., Vargas, E., Santos, L. S., Durán-Lara, E. F., "Preparation of Hydrogel/Silver Nanohybrids Mediated by Tunable-Size Silver Nanoparticles for Potential Antibacterial Applications". *Polymers*, 11 (2019) 716.
68. Kim, J. S., Kuk, E., Yu, K., Kim, J. H., Park, S. J., Lee, H. J., Kim, S. H., Park, Y. K., Park, Y. H., Hwang, C. Y., Kim, Y. K., Lee, Y. S., Jeong, D. H., Cho, M. H., "Antimicrobial effects of silver nanoparticles", *Nanomedicine*, 3 (2007) 95–101.
69. Prabhu, S., Poulose, E. K., "Silver nanoparticles: mechanism of antimicrobial action, synthesis, medical applications, and toxicity effects", *Int. Nano. Lett*. 2 (2012) 32-42.
70. Shrivastava, S., Bera, T., Roy, A., Singh, G., Ramachandrarao, P., Dash, D., "Characterisation of enhanced antibacterial effects of novel silver nanoparticles", *Nanotechnology*, 18 (2007) 1-9.